Rapid Communications

Homoclinic chaos and its organization in a nonlinear optics model

Krishna Pusuluri*
Neuroscience Institute, Georgia State University, Petit Science Center, 100 Piedmont Avenue, Atlanta, Georgia 30303, USA

Andrey Shilnikov†
Neuroscience Institute, and Department of Mathematics and Statistics, Georgia State University, Petit Science Center, 100 Piedmont Avenue, Atlanta, Georgia 30303, USA

(Received 4 June 2018; published 30 October 2018)

We developed a powerful computational approach to elaborate on the onset mechanisms of deterministic chaos due to complex homoclinic bifurcations in diverse systems. Its core is the reduction of phase space dynamics to symbolic binary representations that lets one detect regions of simple and complex dynamics as well as fine organization structures of the latter in parameter space. Massively parallel simulations shorten the computational time to disclose highly detailed bifurcation diagrams to a few seconds.

DOI: 10.1103/PhysRevE.98.040202

Dyson states that "new directions in science are launched by new tools much more often than by new concepts" [1]. A breakthrough discovery of deterministic chaos in (infrared gas) lasers in nonlinear optics was established and pioneered both theoretically and experimentally a long time ago [2–6]. Recent developments in semiconductor lasers and nano-optics have stimulated the latest advances in optical synchronization and photonic integrated circuits for the needs of cryptography [7–12].

Nowadays, a real advance in deterministic nonlinear science stimulating the progress of cutting-edge engineering is hardly possible without significantly deepening the knowledge and beneficial usage of complex elements borrowed from dynamical systems theory. This in turn is hardly possible without the development and incorporation of new mathematical and computational tools, including for parallel graphics processing unit (GPU) based platforms.

In this Rapid Communication we demonstrate how our toolkit, called "deterministic chaos prospector (DCP)," along with the bifurcation-parameter continuation technique, lets one quickly and fully disclose and elaborate on the origin of complex chaotic dynamics in a six-dimensional (6D) model of a resonant three-level optically pumped laser (OPL) [13,14]. In addition to the simple dynamics associated with stable equilibria and periodic orbits, it reveals a broad range of bifurcation structures that are typical for many ordinary differential equation (ODE) models from nonlinear optics and other diverse applications [15–21]. These include homoclinic orbits and heteroclinic connections between saddle equilibria that are the key building blocks of deterministic chaos in most systems. Their bifurcation curves with characteristic spirals around the terminal (T) points along with other codimension-2 points are the organizing centers that shape the regions of complex and simple dynamics in the parameter space of such systems. The detection of these bifurcations has long remained the state of the art involving a meticulous and time-consuming parameter continuation technique to disclose a few sparse elements of the otherwise rich and fine organization of the bifurcation set. We note that while the brute-force approach based on the evaluation of Lyapunov exponents can effectively locate stability windows within regions of chaos [22,23], it fails to disclose these essential structures that are imperative for the exhaustive understanding of complex dynamics and their origin. We will demonstrate how our approach, exploiting the sensitivity of deterministic chaos and its symbolic representation using binary sequences combined with Lempel-Ziv complexity algorithms [24], can effectively reveal regions of complex, structurally unstable, and simple stable dynamics in this and other systems.

The three-level optically pumped laser model [13,14] is given by

$$\begin{aligned}
\dot{\beta} &= -\sigma\beta + 50p_{23},\\
\dot{p}_{21} &= -p_{21} - \beta p_{31} + aD_{21},\\
\dot{p}_{23} &= -p_{23} + \beta D_{23} - ap_{31},\\
\dot{p}_{31} &= -p_{31} + \beta p_{21} + ap_{23},\\
\dot{D}_{21} &= -b\big(D_{21} - D_{21}^{0}\big) - 4ap_{21} - 2\beta p_{23},\\
\dot{D}_{23} &= -b\big(D_{23} - D_{23}^{0}\big) - 2ap_{21} - 4\beta p_{23},
\end{aligned} \tag{1}$$

with parameters a, β, and $\sigma = \{1.5; 10\}$ being the Rabi flopping quantities representing the electric field amplitudes at pump and emission frequencies, and the cavity loss parameter, respectively; b is the ratio of population to polarization decay rates; p_{ij} is the normalized density matrix element corresponding to the transitions between levels i and j, while D_{ij} is the population difference between the ith and jth levels. Note that Eqs. (1) are $\mathbb{Z}_2$ symmetric under the involution $(\beta, p_{21}, p_{23}, p_{31}, D_{21}, D_{23}) \leftrightarrow (-\beta, p_{21}, -p_{23}, -p_{31}, D_{21}, D_{23})$, which is typical for Lorenz-like systems [17,25]. Depending on the (a, b) values,

*pusuluri.krishna@gmail.com
†ashilnikov@gsu.edu

 ©2018 American Physical Society

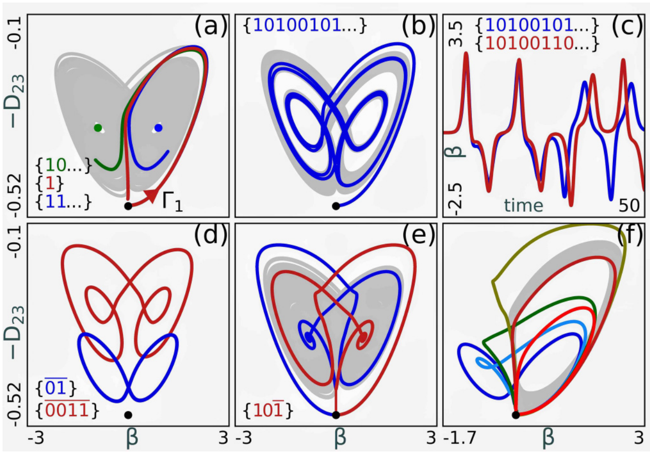

FIG. 1. (a) $(\beta, -D_{23})$ phase space projection showing the primary homoclinic orbit (red, coded as {1}) splitting leftward/rightward (green/blue, $\{10\ldots\}$ or $\{11\ldots\}$) when the separatrix Γ_1 misses the saddle O (black dot) after completing a single turn around the saddle focus C^+, with the Lorenz attractor (in gray) in the background. (b) Chaotic transient of Γ_1 generating a binary sequence starting with $\{10100101\ldots\}$. (c) Time evolutions of the β coordinate of Γ_1 [in (b)] and of a close trajectory (red), and their binary codes, before they diverge. (d) Two stable symmetric POs coded as $\{\overline{01}\}$ and $\{\overline{0011}\}$. (e) Heteroclinic connections (red $\{10\overline{1}\}$, blue symmetric counterpart) at the T_1 point (Fig. 2). (f) Samples (P_j) of the primary homoclinic orbit morphing to a double loop after the inclination flip IF_1 on the curve H_0 in the (a, b)-parameter plane in Fig. 2; here, $\sigma = 1.5$.

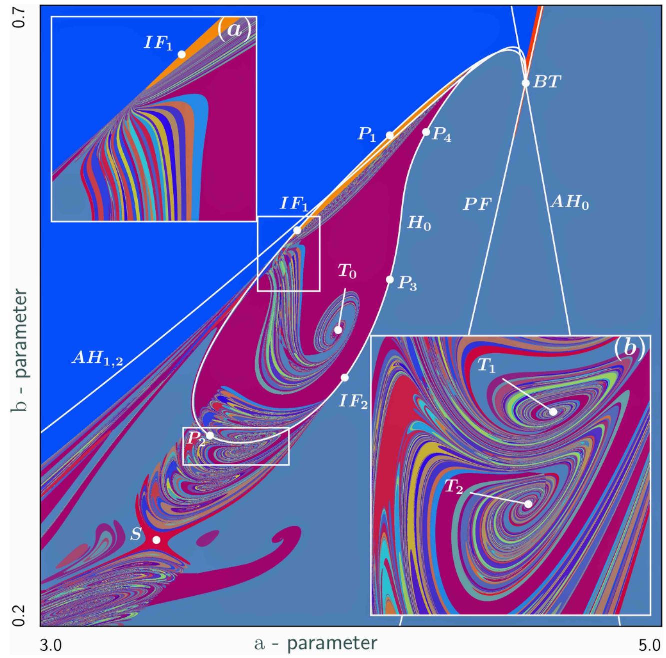

FIG. 2. (a, b)-parameter sweep of [5–12] length reveals an abundance of homoclinic bifurcations emerging from two cod-2 points, IF_1 and IF_2, on H_0, that correspond to the primary homoclinic butterfly of saddle O, along with self-similar characteristic spirals around the T points, labeled $T_{0,1,2}$, corresponding to distinct heteroclinic cycles between O and saddle foci $C^\pm$. Cod-2 Bogdanov-Takens (BT) unfolding includes Andronov-Hopf AH_0, $\mathrm{AH}_{1,2}$ and pitchfork PF bifurcation curves for O and $C^\pm$, respectively; here, $\sigma = 1.5$.

the laser model (1) has either a single nonlasing steady state O or an extra pair of equilibria $C^\pm$ [Fig. 1(a)], emerging as O loses stability through a pitchfork (PF) bifurcation and becomes a saddle. All three steady states can independently undergo supercritical Andronov-Hopf (AH) bifurcations [curves labeled with AH_0 and $\mathrm{AH}_{1,2}$ in the $(a,\ b)$-parameter plane in Fig. 2] giving rise to stable periodic orbits (POs) in the phase space of the laser model (1). Both structural and dynamical instability in the model are due to an abundance of homoclinic bifurcations (HB) of the saddle O, whose one-dimensional (1D) unstable separatrix Γ_1 (and the symmetric counterpart Γ_2) densely fills out the two spatially symmetric wings of the butterfly-shaped strange attractor [Figs. 1(a) and 1(e)] [25]. As parameters are varied, Γ_1 constantly and unpredictably changes its flip-flop switching patterns within the Lorenz attractor. These patterns change whenever Γ_1 comes back to O to undergo a homoclinic bifurcation. This observation is the core for the proposed symbolic approach that converts chaotic and periodic patterns of Γ_1 around the equilibria $C^\pm$ into binary sequences $\{k_n\}$ as follows:

$$k_n = \begin{cases} 1, & \text{when the separatrix } \Gamma_1 \text{ turns around } C^+, \\ 0, & \text{when the separatrix } \Gamma_1 \text{ turns around } C^-. \end{cases}$$

As such, the periodic sequence $\{111\ldots\}$, or $\{\overline{1}\}$, corresponds to Γ_1 converging to the equilibrium state C^+ or a periodic orbit emerging from it through AH bifurcation, while the sequence $\{100\ldots\}$ or $\{1\overline{0}\}$ corresponds to Γ_1 converging to C^- and so forth. Wherever small parameter variations do not change Γ_1 progressions and hence their binary representations, the system demonstrates structurally stable dynamics, which can be due to stable equilibria or periodic orbits (POs), such as the symmetric POs turning once (figure-8 shaped) or twice around C^- and C^+ in Fig. 1(d), with corresponding binary sequences $\{\overline{01}\}$ and $\{\overline{0011}\}$, respectively. An aperiodic binary sequence is associated with chaotic dynamics that is characterized by the sensitive dependence on small parameter variations that change Γ_1 progressions and the corresponding symbolic sequences [Fig. 1(c)]. Changes occur at homoclinic bifurcations when Γ_1 comes back to saddle O. The primary homoclinic orbit [shown in Figs. 1(a) and 1(f)] coded with a finite sequence {1} separates periodic patterns coded as $\{\overline{1}\}$ and $\{1\overline{0}\}$. It occurs on the bifurcation curve H_0 in the (a, b)-parameter plane in Fig. 2. There are two special points labeled as IF_1 and IF_2 on H_0 that correspond to the so-called inclination-flip (IF) bifurcation of codimension-2 [26]. Its feature is that it gives rise to instant homoclinic chaos in the phase space and complex bifurcation structures in the parameter space of the system. With our computational-symbolic toolkit we can clearly and quickly identify such bifurcations and their fine organizations in the parameter space along with regions of chaotic and regular dynamics. First, we define a formal power series $P(N)$ for a finite binary sequence $\{k_n\}$ of length N, after omitting the first j symbols for initial transients of the separatrix Γ_1 or any other trajectory, as follows,

$$P(N) = \sum_{n=j+1}^{j+N} \frac{k_n}{2^{(N+j+1)-n}}. \tag{2}$$

By construction, the range of $P(N)$ is [0, 1], including the sequences $\{\bar{0}\}$ and $\{\bar{1}\}$ (in the limit as $N \to \infty$). For example, $P(8)$ for the aperiodic sequence {10100101} generated by Γ_1 in Fig. 1(b), with $j = 0$ and $N = 8$, is given by $P(8) = 1/2^8 + 0/2^7 + 1/2^6 + 0/2^5 + 0/2^4 + 1/2^3 + 0/2^2 + 1/2^1 = 0.644\,531\,25$.

The P quantities are used as invariants to discriminate or conjugate finite progressions of the separatrix Γ_1 of the saddle against each other to identify and trace down corresponding bifurcation curves in the parameter space. Moreover, the quantities generated from long periodic and aperiodic binary sequences let us efficiently detect regions of regular and chaotic dynamics, respectively. Keeping σ fixed at 1.5 or 10, we (1) vary a and b to get a biparametric sweep on a 2000×2000 grid, (2) to follow Γ_1 progressions, (3) generating binary sequences $\{k_n\}$ that (4) result in $P(N)$ quantities. Next, (5) we color map all found $P(N)$ values onto the parameter plane, where regions are identified by their equivalent colors, and the borderlines between adjacent regions correspond to homoclinic bifurcation curves. The color map differentiates between $P(N)$ values grouped into 2^{24} bins with preset RGB-color values. Such sweeps can be massively parallelized by running separate threads on a GPU. For example, the sweep of [5–12] length, i.e., with the first five symbols omitted, shown in Fig. 2 takes about 8 s to run on a Tesla K40 GPU by Nvidia. It is superimposed with the curves, obtained by parametric continuation, corresponding to pitchfork (PF), Andronov-Hopf (AH_0 and $AH_{1,2}$ for O and $C^{\pm}$), and the primary homoclinic (H_0) bifurcations all originating from the codimension-2 Bogdanov-Takens point (BT) [26]. Figure 1(f) shows how the primary homoclinic loop transmutes into a double loop along the curve H_0. The sweep reveals the way the inclination-flip IF_1 and IF_2 points give rise to jets of homoclinic bifurcation curves spiraling to various self-similar cod-2 Bykov terminal T points, including T_0 and T_1, that correspond to heteroclinic connections linking the saddle O with saddle foci C^+, C^- and generating periodic sequences $\{1\bar{0}\}$, $\{10\bar{1}\}$ [Fig. 1(e)], respectively.

Figure 3(a) shows that with longer sequences we can obtain more detailed sweeps disclosing multiple T points of smaller scales near the saddle point S that are not seen in Fig. 2. These spiral structures around the T points (identical to T_2^1 and T_2^2 in Fig. 4) morph into closed loops [as those shown in Fig. 3(c)] after collapsing into the saddle as the σ parameter is varied (shown in movie 1 in the Supplemental Material [27].) Figures 3(b) and 3(d) present a sweep of [100–123] length, i.e., after skipping the first 100 transient symbols. Here, regions with solid colors of constant $P(23)$ values represent the stability windows corresponding to simple (periodic) Morse-Smale dynamics, whereas multicolored noisy regions refer to structurally unstable chaotic dynamics, as described later.

The (a, b) sweep of [2–9] length in Fig. 4 demonstrates the intrinsic rearrangement of the bifurcation constituents of complexity for a different cut at $\sigma = 10$. Here, the secondary inclination-flip point (IF_2) gives rise to loci of outgoing homoclinic curves that are redirected by a saddle point (S), and spiral onto multiple T points. The heteroclinic connections at the T points T_0–T_3 are given by $\{1\bar{0}\}$, $\{10\bar{1}\}$, $\{11\bar{0}\}$, and $\{\bar{1}\}$, respectively. The T points T_2^1 and T_2^2, separated by the saddle

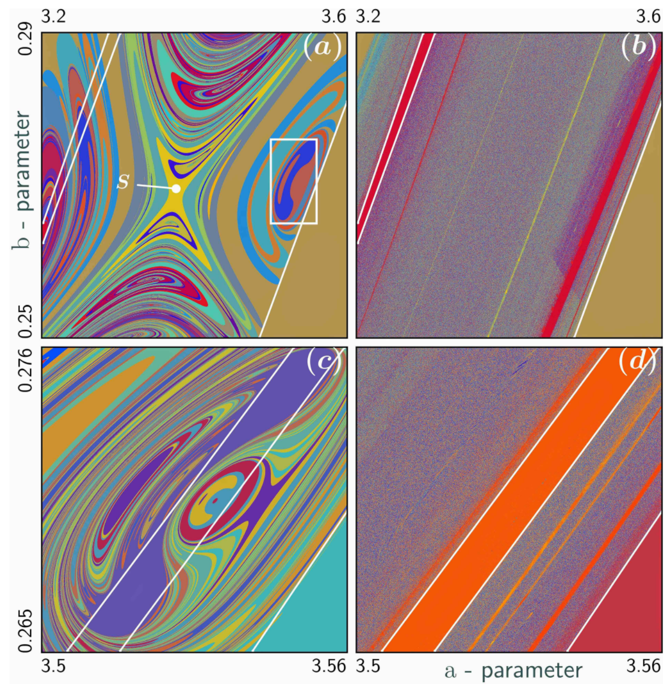

FIG. 3. (a) Short [8–15] and (b), (d) long [100–123] length (a, b) sweeps reveal fine self-similar organization of homo- and heteroclinic bifurcations underlying the regions of chaotic and regular dynamics of model (1) for $\sigma = 1.5$. A small area (white box) in (a) is magnified with a longer [15–22] sweep in (c). (b) and (d) reveal stability windows (solid colors) within "noisy" regions of structurally unstable chaos; white lines demarcate boundaries of some stability windows.

S, correspond to the same heteroclinic connection $\{11\bar{0}\}$. Note that here the primary homoclinic curve spirals onto the primary T point T_0. The T point T_3 belongs to the stability window dominated by the symmetric figure-8 periodic orbit [Fig. 1(d)] in the long run. The semiannular structures around C are, in fact, the remnants of the spirals around T_3, where the other halves of the spirals are disintegrated by the stable periodic orbit existing near T_3. With small σ variations, T_3 crosses over the stability boundary near C, so that both ends of the semiannular structures merge to complete spirals around T_3 (as demonstrated in movie 2 in the Supplemental Material [27].) Meanwhile, T points T_2^1 and T_2^2 merge with the saddle S to transform into concentric cycles. These structures in the 2D sweeps are the contour curves of the corresponding surfaces in the 3D (a, b, σ)-parameter space of the model (1). Figure 5 demonstrates this saddle as the critical point of the 3D surface shaped as a hyperbolic paraboloid, constructed using 8×10^9 trajectories in the parameter space. Depending on the particular σ cuts, the contour lines of the bent scroll-shaped surfaces may resemble spirals or closed concentric circles in the projections in Figs. 2–4.

While a detailed sweep for short-term transient dynamics lets us reveal the underlying homoclinic bifurcations, longer sweeps omitting initial transients are designed to localize stability windows corresponding to regular dynamics and regions of chaotic dynamics in the parameter space. We implemented two algorithms into our computational DCP toolkit

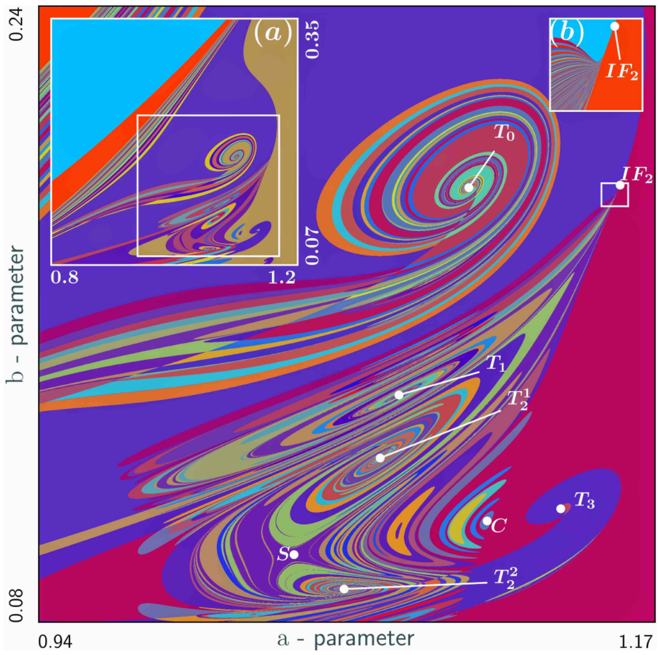

FIG. 4. [2–9] length sweep discloses organization of homo/heteroclinic bifurcations originating from cod-2 inclination flip IF_2 and multiple T points: Primary T_0 coded as $\{1\overline{0}\}$, secondary T_1 as $\{10\overline{1}\}$, and a pair $T_2^1 - T_2^2$ with code $\{11\overline{0}\}$ separated by a saddle (S) in the (a, b)-parameter plane; here, $\sigma = 10$. Inset (a) shows a larger (a, b) sweep of [1–7] length; (b) [16–23]-long sweep depicts dense loci of homoclinic bifurcation curves originating from IF_2.

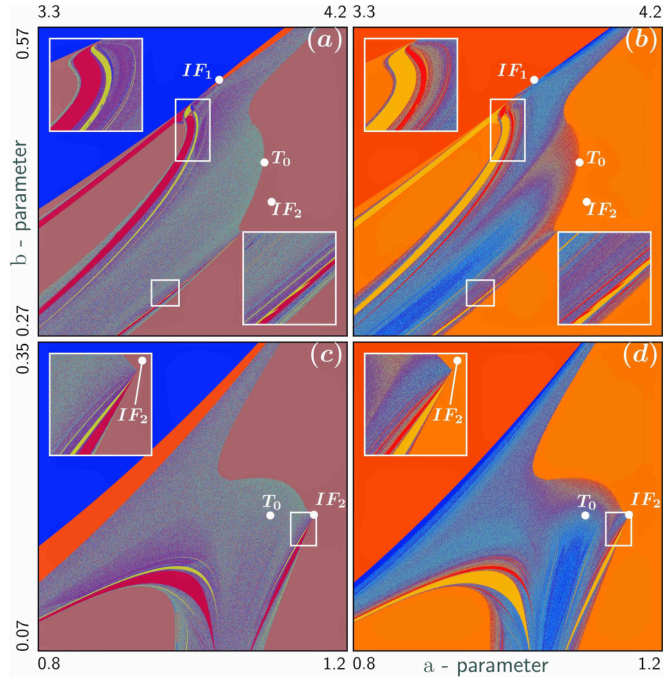

FIG. 6. Long [1000–1999]-length sweeps to detect a multiplicity of stability windows [solid colors; dark red due to stable PO $\{\overline{0011}\}$ in Fig. 1(d)] within noisy/multi-color regions of chaos adjacent to IF_1 and IF_2 points in the (a, b)-parameter plane using PC algorithm in (a) and (c), and LZ-complexity in (b) and (d). Sweeps at $\sigma = 1.5$ (a,b) and $\sigma = 10$ (c,d) to compare with Fig. 2 and 4.

to classify such regions depending on whether or not the corresponding binary sequences of the solutions are periodic for the given parameter values. The first algorithm based on Eq. (2) includes periodicity correction (PC) to identify the periodic structure within a binary sequence and to normalize it to its smallest valued circular permutation. For example, the symmetric figure-8 periodic orbit in Fig. 1(d) is coded with $\{\overline{01}\}$ not with $\{\overline{10}\}$. The second algorithm utilizes the Lempel-Ziv-76 (LZ) compression [24], to determine the normalized complexity (the number of words in vocabulary per sequence length) of the binary sequence. The LZ compression algorithm scans a sequence from left to right and adds a new word to the vocabulary every time a previously unencountered substring is detected. Since all circular permutations of a periodic orbit have the same complexity, with this approach we can also detect stability windows amidst structurally unstable chaotic regions. This approach requiring only one solution per parameter set complements more expensive computational approaches based on the evaluations of the largest or several Lyapunov exponents.

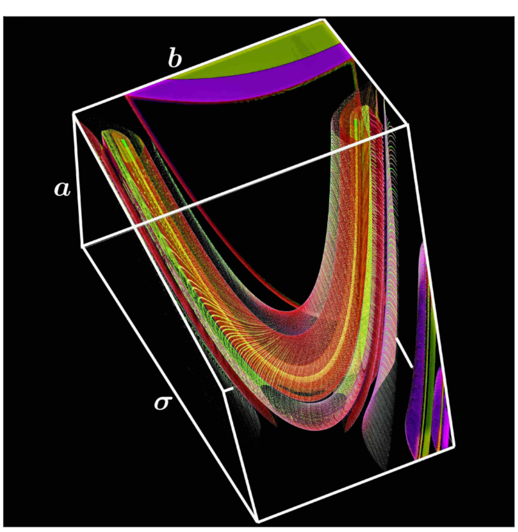

FIG. 5. Fragment of the 3D (a, b, σ)-parameter space (based on a $2000 \times 2000 \times 2000$ grid) depicting various nested elliptic and hyperbolic paraboloids whose contour curves appear as spirals around T points, and/or concentric circles near saddles in the biparametric sweeps in Figs. 2–4.

Figure 6 represents the biparametric [1000–1999]-long sweeps to identify regions of simple and complex dynamics in model (1); here, insets (a)/(c) and (b)/(d) represent the PC- and LZ-algorithm-based sweeps, respectively. Regions of solid monotone colors correspond to the stability windows with stable equilibrium states and periodic orbits, while multi-colored noisy regions indicate that the dynamics is structurally unstable and chaotic. The sweeps in Figs. 6(a) and 6(b) (at $\sigma = 1.5$) are superimposed with the primary and secondary inclination-flip points IF_1 and IF_2 along with the primary T point T_0 located next to the boundary between the regions of chaotic and stable periodic dynamics. They reveal multiple stability windows adjacent to IF_1 and IF_2 (magnified insets), including the wide one (in dark red) corresponding to a stable periodic orbit $\{\overline{0011}\}$ [shown in Fig. 1(d)]. This approach can clearly identify distinct periodic orbits and their stability windows mapped by different colors. Note that the same stability windows (indicated with the same colors) emerge near both IF_1 and IF_2 in reversed order. The sweeps in Figs. 6(c) and 6(d) (at $\sigma = 10$) depict the primary T point T_0 located inside the region of chaotic dynamics, and the stability windows accumulating to IF_2. We note that the PC algorithm lets one detect and identify a variety of stable periodic orbits efficiently even with short symbolic sequences [see Figs. 3(b) and 3(d)] compared to quite long sequences required by the LZ algorithm that is better suited for the detection of chaotic regions. This observation suggests the order to analyze the given sequence is to first run it through the PC algorithm to detect periodic orbits, and next through the LZ algorithm to detect the complexity of aperiodic strings on a GPU. Other future enhancements of the DCP toolkit are to include the search algorithms for bifurcations of equilibrium states and periodic orbits such as period doubling.

In conclusion, we have demonstrated the proficiency of this symbolic toolkit for computational studies of both transient and long-term solutions to analyze the bifurcation mechanisms underlying the onset of chaotic and regular dynamics in the phase and parameter spaces of the given OPL model and similar deterministic systems.

This work was in part funded by NSF Grant No. IOS-1455527, RSF Grant No. 14-41-00044 at the Lobachevsky University of Nizhny Novgorod, and MESRF Project No. 14.740.11.0919. We thank GSU's Brains and Behavior initiative for fellowship and pilot grant support, NVIDIA corporation for the donation of Tesla K40 GPU, and the members of Shilnikov's NeurDS laboratory for helpful discussions.

[1] F. J. Dyson, *Imagined Worlds* (Harvard University Press, Cambridge, MA, 1998).
[2] H. Haken, Phys. Lett. A **53**, 77 (1975).
[3] H. Haken, *Laser Light Dynamics* (North-Holland, Amsterdam, 1985).
[4] C. Weiss and H. King, Opt. Commun. **44**, 59 (1982).
[5] C. Weiss, W. Klische, P. Ering, and M. Cooper, Opt. Commun. **52**, 405 (1985).
[6] C. O. Weiss and J. Brock, Phys. Rev. Lett. **57**, 2804 (1986).
[7] L. M. Pecora and T. L. Carroll, Phys. Rev. Lett. **64**, 821 (1990).
[8] Y. Liu, N. Kikuchi, and J. Ohtsubo, Phys. Rev. E **51**, R2697 (1995).
[9] G. D. Vanwiggeren and R. Roy, Science **279**, 1198 (1998).
[10] A. Argyris, M. Hamacher, K. E. Chlouverakis, A. Bogris, and D. Syvridis, Phys. Rev. Lett. **100**, 194101 (2008).
[11] J. Ohtsubo, *Semiconductor Lasers: Stability, Instability and Chaos*, Springer Series in Optical Sciences Vol. 111 (Springer, Berlin, 2012).
[12] M. Naruse, S.-J. Kim, M. Aono, H. Hori, and M. Ohtsu, in *European Quantum Electronics Conference* (Optical Society of America, Washington, DC, 2015), p. EG_P_15.
[13] J. V. Moloney, J. S. Uppal, and R. G. Harrison, Phys. Rev. Lett. **59**, 2868 (1987).
[14] W. Forysiak, J. Moloney, and R. Harrison, Physica D **53**, 162 (1991).
[15] R. Barrio, A. Shilnikov, and L. Shilnikov, Int. J. Bifurcation Chaos Appl. Sci. Eng. **22**, 1230016 (2012).
[16] T. Xing, J. Wojcik, R. Barrio, and A. Shilnikov, in *International Conference on Theory and Application in Nonlinear Dynamics (ICAND 2012)* (Springer, Berlin, 2014), pp. 129–140.
[17] T. Xing, R. Barrio, and A. Shilnikov, Int. J. Bifurcation Chaos Appl. Sci. Eng. **24**, 1440004 (2014).
[18] T. Xing, J. Wojcik, M. Zaks, and A. L. Shilnikov, in *Chaos, Information Processing and Paradoxical Games: The Legacy of J. S. Nicolis*, edited by G. Nicolis and V. Basios (World Scientific, Singapore, 2015).
[19] K. Pusuluri, A. Pikovsky, and A. Shilnikov, in *Advances in Dynamics, Patterns, Cognition* (Springer, Berlin, 2017), pp. 41–60.
[20] J. G. Freire, R. Meucci, F. T. Arecchi, and J. A. Gallas, Chaos **25**, 097607 (2015).
[21] F. Marino, M. Ciszak, S. F. Abdalah, K. Al-Naimee, R. Meucci, and F. T. Arecchi, Phys. Rev. E **84**, 047201 (2011).
[22] J. A. Gallas, Int. J. Bifurcation Chaos Appl. Sci. Eng. **20**, 197 (2010).
[23] R. Barrio, F. Blesa, S. Serrano, and A. Shilnikov, Phys. Rev. E **84**, 035201 (2011).
[24] A. Lempel and J. Ziv, IEEE Trans. Inf. Theory **22**, 75 (1976).
[25] V. S. Afraimovich, V. Bykov, and L. P. Shilnikov, Akad. Nauk SSSR Dokl. **234**, 3369 (1977) [Sov. Phys. Dokl. **22**, 253 (1977)].
[26] L. Shilnikov, A. Shilnikov, D. Turaev, and L. Chua, *Methods of Qualitative Theory in Nonlinear Dynamics*, Vols. 1–2 (World Scientific, Singapore, 1998/2001).
[27] See Supplemental Material at http://link.aps.org/supplemental/10.1103/PhysRevE.98.040202 for numerical details and movies of the 3D sweeps.